Materials & Design 129 (2017) 116–124

Contents lists available at ScienceDirect

Materials & Design

journal homepage: www.elsevier.com/locate/matdes

Scaling aerosol assisted chemical vapour deposition: Exploring the relationship between growth rate and film properties

Michael J. Powell, Dominic B. Potter, Rachel L. Wilson, Jawwad A. Darr, Ivan P. Parkin, Claire J. Carmalt*

Department of Chemistry, University College London, 20 Gordon Street, London WC1H 0AJ, UK

ARTICLE INFO

Keywords:
Aerosol assisted CVD
Transparent conducting oxides
Materials processing

ABSTRACT

Thin films of fluorine doped tin oxide were deposited, by an aerosol assisted chemical vapour deposition route, to study the effect of scaling the growth rate. The effect of precursor concentration on the growth rate of the films and the properties of deposited films were compared. The films were characterised by X-ray diffraction, scanning electron microscopy, UV/vis spectroscopy, X-ray photoelectron spectroscopy and Hall effect measurements. A maximum film growth rate of ca. 100 nm min^{-1} was observed, which is significantly faster than previously reported aerosol assisted studies. This method shows the ability of aerosol assisted methods to deliver high growth rates whilst maintaining the ease of doping and control over stoichiometry.

GRAPHICAL ABSTRACT

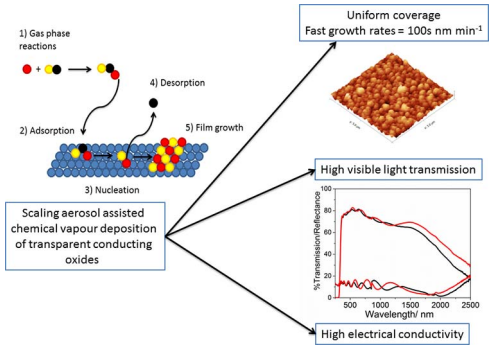

1. Introduction

Chemical vapour deposition (CVD) routes are widely employed in the production of thin films for industrial applications, such as; solar cells [1–3], flat screen displays [4,5], self-cleaning surfaces [6–9] and transparent conducting oxides (TCOs) [10–12]. For many of these applications, atmospheric pressure CVD (APCVD) is the route employed to synthesise the thin film coatings. This methodology has a few drawbacks, one of which is the need to have volatile precursors [4]. This limits the range of available precursors, with metal chlorides being commonly employed, resulting in the need to process the exhaust gases to remove HCl/Cl_2 [13]. A second major drawback of APCVD routes is the ability to dope the materials to improve the properties. Here, as well as the availability of suitable precursors, the main issue is controlling the incorporation of the dopant into the material. This is not a trivial matter, as fluid dynamics control the level of doping in the structure [14]. Finally, tailoring of the material morphology is also difficult to achieve in many APCVD processes.

Even with the above limitations, APCVD is favoured for certain industrial processes as it can deliver uniform conformal coatings, with

* Corresponding author.
E-mail address: c.j.carmalt@ucl.ac.uk (C.J. Carmalt).

http://dx.doi.org/10.1016/j.matdes.2017.05.017
Received 6 January 2017; Received in revised form 5 May 2017; Accepted 8 May 2017
Available online 11 May 2017

high growth rates (up to 100s nm s^{-1}) over large substrate areas [15]. This means that in industrial processes, many 100s of metres of material can be coated per hour. It would be advantageous to develop other routes towards industrial thin film production that allow for the same abilities, but reduce the drawbacks mentioned above. There are several synthetic routes that could be used for this, such as spray-coating and aerosol assisted chemical vapour deposition (AACVD). Of these two, AACVD would be the best suited to being incorporated into current industrial plants for thin film depositions, as the aerosol can be generated and carried to the processing line using the existing facilities.

AACVD relies on the ability to produce an aerosol from a solution containing a suitable metal precursor. This aerosol is then carried to the reaction chamber by a carrier gas, where it passes over a heated substrate resulting in nucleation, reaction and film growth. By being solution based, there are many more available precursors for AACVD synthesis than APCVD. The ability to control the dopant incorporation is also much easier, as the dopant incorporation is directly proportional to the concentration of dopant in the precursor solution [16,17]. AACVD also allows for better tailoring of morphology, as surfactants and nanoparticles can be included in the precursor solution which can then change the morphology present in the deposited film [18–20]. Recently Yamada et al. have shown that 'mist' CVD methods can be used to optimise materials for physical vapour deposition [21].

A wide variety of metal oxide thin films have been synthesised by AACVD methods making this an ideal technique to deposit functional thin film materials. Noor et al. were able to deposit thin films of F-doped SnO_2 (FTO) by AACVD with resistivity values as low as $4 \times 10^{-4}\,\Omega\square^{-1}$ [5]. The growth rate for these films was ca. 10 nm min^{-1}. Edusi et al. synthesised thin films of TiO_2 for photocatalytic applications [22]. In this study the growth rate was between 2 and 10 nm min^{-1}. Chadwick et al. synthesised composite thin films of TiO_2/SnO_2 by AACVD [23]. In this study a maximum growth rate of between 15 and 20 nm min^{-1} was observed.

One of the current drawbacks of AACVD is the relatively slow growth rates, with typical lab-scale AACVD reactions giving growth rates of ca. 10 nm min^{-1}. This would be clearly too slow for many industrial applications and before the benefits of aerosol assisted processes can be realised, the ability to deliver fast growth rates must be demonstrated. A Web of Science search showed that there have been over 340 publications in the past 5 years where AACVD has been used to synthesise functional thin films, however, to the best of our knowledge, there has yet to be a systematic study on scaling AACVD.

Outlined in this paper is a route towards scaling AACVD for industrial uses. We will focus on the ability to increase the growth rate from 10s of nm min^{-1} to 100s of nm min^{-1}. Coupled to this, we will also explore the relationship between the film growth rate and the properties observed in the deposited films and establish rules for scaling aerosol assisted synthetic techniques. Finally, we explore whether increasing the fluorine concentration can deliver superior electrical properties whilst maintaining high visible light transmission in the deposited films. We have chosen FTO as our system for this series of experiments, as it is a well-characterised transparent conducting oxide (TCO) material and so is ideal for determining the effectiveness of this process.

2. Experimental

All chemicals were used as bought: monobutyltin trichloride (95%, Sigma-Aldrich), ammonium fluoride (98%, Sigma-Aldrich) and methanol (99.9%, Fisher). Compressed air was used as supplied from BOC. The glass substrate used for depositions was 3.2 mm thick plain float glass with a 50 nm thick SiO_2 barrier layer (Pilkington/NSG).

2.1. Thin film synthesis

AACVD thin film depositions were carried out as detailed elsewhere

Table 1
Sample descriptions and refinement of lattice parameters for FTO thin films deposited. The F:Sn ratio in the precursor solution was varied to determine if the electrical properties of the deposited films could be further improved. Deposition times were fixed at 5 min with air used as the carrier gas for all depositions.

Sample no.	Sample description	F:Sn ratio in precursor solution	Lattice parameter a = b (Å)	Lattice parameter c (Å)	Cell volume ($Å^3$)	Film thickness d/(μm)
1	Thin film of F:SnO_2 deposited from 0.2 mol dm^{-3} monobutyltin trichloride in methanol with 15 mol% ammonium fluoride	1:6.7	4.7377(5)	3.188(1)	71.57(3)	0.15
2	Thin film of F:SnO_2 deposited from 0.2 mol dm^{-3} monobutyltin trichloride in methanol with 30 mol% ammonium fluoride	1:3.3	4.7383(4)	3.190(1)	71.62(2)	0.15
3	Thin film of F:SnO_2 deposited from 0.5 mol dm^{-3} monobutyltin trichloride in methanol with 15 mol% ammonium fluoride	1:6.7	4.7411(6)	3.1914(5)	71.74(3)	0.40
4	Thin film of F:SnO_2 deposited from 0.5 mol dm^{-3} monobutyltin trichloride in methanol with 30 mol% ammonium fluoride	1:3.3	4.7378(2)	3.1894(4)	71.59(1)	0.40
5	Thin film of F:SnO_2 deposited from 1.0 mol dm^{-3} monobutyltin trichloride in methanol with 15 mol% ammonium fluoride	1:6.7	4.7410(7)	3.1878(6)	71.65(3)	0.50
6	Thin film of F:SnO_2 deposited from 1.0 mol dm^{-3} monobutyltin trichloride in methanol with 30 mol% ammonium fluoride	1:3.3	4.7391(3)	3.1867(8)	71.57(2)	0.50
7	Thin film of F:SnO_2 deposited from 2.0 mol dm^{-3} monobutyltin trichloride in methanol with 15 mol% ammonium fluoride	1:6.7	4.7356(4)	3.1867(7)	71.47(2)	0.50
8	Thin film of F:SnO_2 deposited from 2.0 mol dm^{-3} monobutyltin trichloride in methanol with 30 mol% ammonium fluoride	1:3.3	4.7374(3)	3.1885(6)	71.56(1)	0.50

[24], as in this study the F-doped SnO_2 thin films were optimised for electrical and optical properties. The carbon block heater comprising the lower half of the reactor was used to maintain the substrate temperature using a k-type thermocouple. Depositions were carried out on Pilkington silica-coated barrier glass (50 nm SiO_2 coated on one side of float glass), with depositions occurring on the atmospheric (silica barrier) side of the glass in order to prevent unwanted leaching of ions from the glass into the thin film [25]. Prior to deposition, the glass substrates were cleaned with soapy water, isopropanol and acetone and were then left to air dry. The substrate was then loaded into the reaction chamber along with a second piece of float glass suspended 8 mm above (silica barrier layer pointing down) to ensure laminar flow during deposition. The AACVD of the fluorine-doped tin oxide (FTO) thin films was achieved by synthesising a precursor solution by dissolving monobutyltin trichloride and ammonium fluoride in methanol, the mol% of the ammonium fluoride (NH_4F) was either 15% or 30% relative to the tin. The monobutyltin trichloride ($^nBuSnCl_3$) precursor concentration was varied between 0.2 and 2 mol dm^{-3}. Sample descriptions and lattice parameters can be found in Table 1. The aerosol was generated by means of a pneumatic collision generation method, using a *TSI Model 3076 Constant Output Atomiser*, which typically generated 0.3 μm-sized aerosol droplets. The aerosol was carried to the reaction chamber by a stream of compressed air, which was kept at a constant pressure of 2 bar during depositions. All films were deposited at 550 °C, as this has been previously shown to give superior TCO properties [5]. Deposition times were fixed at 5 min. After depositions, the films were allowed to cool naturally to room temperature. Deposited films were handled and stored in air. All samples were synthesised multiple times to determine the repeatability of the process, the data presented is typical for the thin films synthesised.

2.2. Thin film characterisation

Scanning electron microscope images were recorded on a *Jeol JSM-6301F* SEM at an acceleration voltage of 5 kV. Atomic force microscopy (AFM) images were recorded using a *Nanosurf easy scan* Atomic Force Microscope, equipped with a 10 μm tip in non-contact mode with oscillating probe. The scan area was 5 μm × 5 μm with 20 nm scan intervals. X-ray diffraction (XRD) patterns were recorded using a *Bruker D8 Discover* X-ray diffractometer using monochromatic Cu $K_{\alpha1}$ and Cu $K_{\alpha2}$ radiation of wavelengths 1.54056 and 1.54439 Å respectively, emitted in an intensity ratio of 2:1 with a voltage of 40 kV and a current of 40 mA. The incident beam angle was 1° and data was collected between 5° and 66° 2θ with a step size of 0.05° at 2.0 s/step. All diffraction patterns obtained were compared with database standards (ICSD). Unit cell volumes and lattice parameters were calculated from the XRD data using unit cell volumes were calculated using GSAS and EXPGUI programs. X-ray photoelectron spectroscopy was conducted on a *Thermo Scientific K-alpha* spectrometer with monochromated Al Kα radiation, a dual beam charge compensation system and constant pass energy of 50 eV (spot size 400 μm). Survey scans were collected in the binding energy range 0–1200 eV. High-resolution peaks were used for the principal peaks of Sn (3d), O (1s), F (1s) and C (1s). Data was calibrated against C1s (285.0 eV). Data was fitted using CASA XPS software. UV/vis spectra were recorded on a *Perkin Elmer Lambda 950* UV/Vis/NIR Spectrophotometer in both transmission and diffuse reflectance mode. A Labsphere reflectance standard was used as a reference for the UV/vis measurements. Room temperature Hall effect measurements were carried out on an *Ecopia HMS-3000* set up in the Van der Pauw configuration. Measurements were taken using a 0.58 T permanent magnet and a current of 1 μA. Tests were carried out on square-cut samples measuring ≈1 × 1 cm. Silver paint (Agar Scientific) was used to form ohmic contacts, which were tested on the in-built software prior to measurement. The Hall effect method was used to find the ρ, μ and n using measured film thickness values as obtained from a *Filmetrics F20* machine operating in reflectance mode, in air, against an as-supplied FTO standard.

3. Results and discussion

3.1. Physical characterisation

For the films deposited, in all cases XRD analysis showed only the presence of the cassiterite phase, which has a tetragonal crystal structure (space group: $P4_2/mnm$), of SnO_2, Fig. 1. There was an obvious change in preferential orientation, with the (200) diffraction plane being favoured by higher precursor concentrations. This is shown most clearly when comparing samples 4 and 6, both of these samples had the same F:Sn ratio of 1:3.3 in the initial precursor solution, however, sample 6 had a tin concentration of 1.0 mol dm^{-3} whilst sample 4 had 0.5 mol dm^{-3} Sn conc. The XRD patterns clearly show that sample 6 had preferred orientation towards the (200) plane, whereas sample 4 showed preferred orientation towards the (101) plane. It has been previously observed that fluorine incorporation leads to the promotion of the (200) diffraction plane [5,26], this suggests that for the samples deposited from 1 and 2 mol dm^{-3} solutions there has been successful incorporation of fluorine. Noor et al. [27] have proposed that there is a halide exchange occurring when a fluoride source is mixed with a metal chloride. This would also allow the fluorine to be in contact with the tin during crystallisation, which could lead to greater fluorine incorporation into the SnO_2 lattice.

The XRD results also suggest that there is another process that also affects the preferential orientation. This could be due to the thickness of the films, with thinner depositions leading to greater strain promoting the (110) plane. This effect has been previously observed by Consonni et al. who observed a change in preferential orientation from (110) to (301) on increasing the thickness of FTO thin films [28].

Film thickness measurements were achieved by ellipsometry measurements, shown in Table 1. It is obvious from the data that as the precursor concentration is increased, the film thicknesses also increase. This relationship is true up to a concentration of 1.0 mol dm^{-3}, however, above this concentration there is no further increase in film thickness. This is attributed to the viscosity of the precursor solution, as at high precursor concentrations it became very viscous and the collision atomiser could no longer draw the solution effectively to be atomised. The increase in film thickness mirrors the change in preferential orientation in the XRD patterns, Fig. 1, and so supports the conclusion that the change in preferential orientation is due to increased film thickness.

As depositions were fixed at 5 min, the maximum film growth rate achieved is 100 nm min^{-1}, which is significantly faster than typical aerosol assisted CVD methods which have growth rates of around 10 nm min^{-1}. The limiting factor was also the ability to deliver the precursor solution to the atomising chamber, which suggests that the growth rates could be further increased.

Refinement of the lattice parameters was conducted on the samples produced, as shown in Table 1. As the F^- ion is smaller than the O^{2-} ion, upon fluorine incorporation into SnO_2, there is a contraction in unit cell volume [29]. Both the 15 and 30 mol% fluorine samples showed the general trend of a contraction in the unit cell volume with increasing Sn concentration, indicating that fluorine incorporation increases with increasing tin concentration. This trend mirrors the change in preferred orientation, from (110) to (200), observed in the XRD patterns for these samples. There was, however, one result that did not fit this pattern, which was for the lower concentration precursor solution (0.2 mol dm^{-3}) with 15% vol. F dopant, which had a cell volume 71.57 $Å^3$ which is substantially reduced when compared to the unit cell volume for higher precursor concentrations. This indicates that at lower concentrations of fluorine and tin in solution, there is initially a superior exchange between the chloride and fluoride.

By combining the results of both the change in preferential orientation, towards the (200), and the reduction in the unit cell

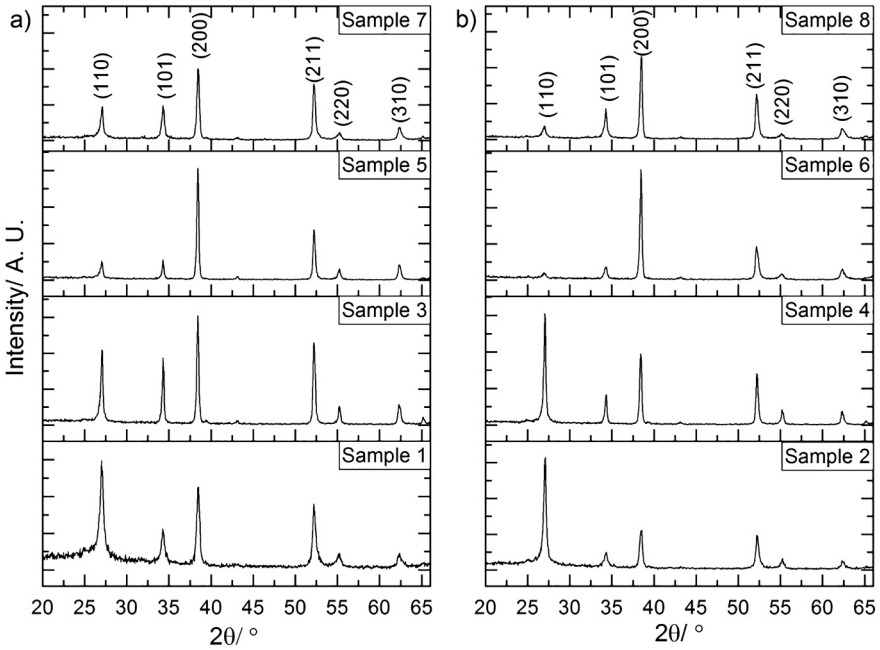

Fig. 1. Typical XRD patterns for a) 15% F (by vol.) SnO_2 thin films and b) 30% F (by vol.) SnO_2 thin films. Sample descriptions can be found in Table 1. All films were deposited by AACVD at 550 °C using compressed air as the carrier gas. All films show the presence of only the cassiterite phase of SnO_2. Films were compared to ICSD standards (ICSD 154960).

volume from the lattice refinement data indicates that fluorine has been successfully incorporated into the thin films. Furthermore, the data indicates that higher levels of fluorine are incorporated when the concentration of the precursors is increased in solution.

The optical properties of the films were characterised by UV/vis spectroscopy, Fig. 2. All films displayed good visible light transmission, with average optical transmission (λ = 400–700 nm) being ≥ 78%, optical properties are summarised in Table 2. Interestingly, the films that displayed optical behaviour associated with low emissivity (low E) coatings, were those that were deposited from the 1.0 mol dm^{-3} solutions, with the films deposited from the 2.0 mol dm^{-3} solutions not displaying this characteristic. Low E coatings are of interest due to their inherent energy saving characteristics when applied to windows as coatings. This effect arises from a large proportion of the near IR wavelengths being reflected due to free carrier absorption effects. Combining the XRD patterns and UV/vis data suggests the desired properties of the films can be tailored by manipulation of the concentration of the precursors in solution with low E coatings favoured by concentrations around 1.0 mol dm^{-3}. This relationship is different from those obtained from atmospheric pressure chemical vapour deposition [30] or spray pyrolysis [31,32], where increasing the amount of precursor available results in films with greater low E characteristics.

To determine the morphology of the deposited films, SEM images were obtained, Fig. 3. Films deposited using a solution concentration of 0.2 mol dm^{-3} did show significant space between at grain boundaries and smaller grain sizes, Fig. 3a), this is attributed to the lower concentration of Sn in solution.

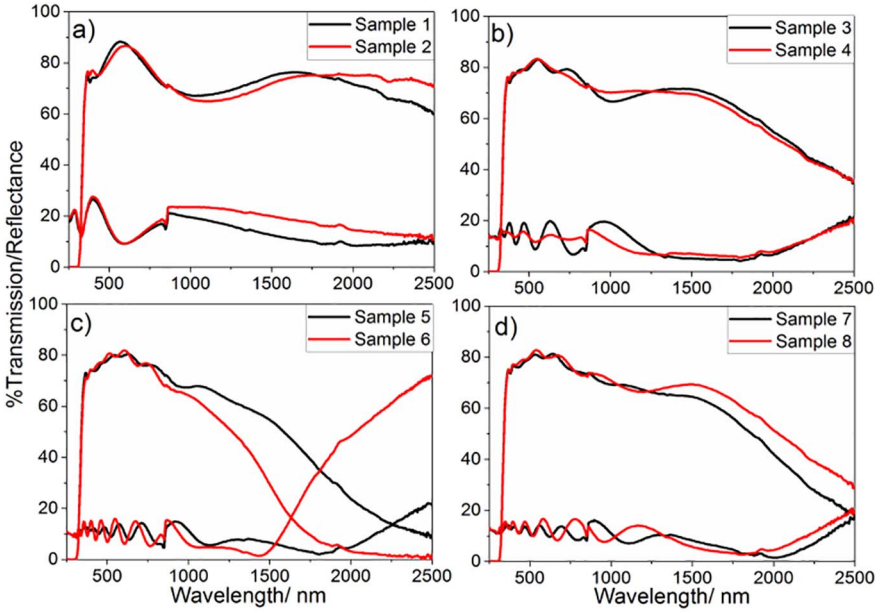

Fig. 2. Typical UV/Vis/NIR spectra for a) 15 and 30% F 0.2 mol dm^{-3} depositions, b) 15 and 30% F 0.5 mol dm^{-3} depositions, c) 15 and 30% F 1.0 mol dm^{-3} depositions and d) 15 and 30% F 2.0 mol dm^{-3} depositions. All films displayed good visible light transmission (≥ 78% transmission between 400 and 700 nm).

Table 2
Table of typical electrical and optical data for all FTO samples synthesised in air by AACVD of $^{n}BuSnCl_3$ and NH_4F in methanol at 550 °C. Deposition time was fixed at 5 mins for every sample. The concentration of the tin and fluorine were varied between samples (see Table 1 for full sample descriptions).

Sample number	F:Sn precursor conc	d/μm	$n/\times 10^{20}$ cm^{-3}	μ/cm^2 V^{-1} s^{-1}	$\rho/\times 10^{-3}$ Ω cm	R_{Sh}/Ω□$^{-1}$	$T_{\lambda,550}$/%	$T_{\lambda,400-700}$/%
1	1:6.7	0.15	0.680	3.52	26.08	1738.7	87.8	83.1
2	1:3.3	0.15	1.503	9.22	4.506	300.4	85.1	82.2
3	1:6.7	0.40	4.579	14.86	0.917	23.0	83.0	79.6
4	1:3.3	0.40	2.941	16.62	1.277	31.9	83.3	80.1
5	1:6.7	0.50	11.84	15.73	0.335	6.7	79.9	78.0
6	1:3.3	0.50	12.26	19.35	0.263	5.3	80.3	78.5
7	1:6.7	0.50	3.061	21.12	0.966	19.9	81.1	79.3
8	1:3.3	0.50	3.173	20.49	0.960	19.2	82.5	80.0
Commercial standards								
TEC™8	0.65	5.3	28	0.52		8.0	83	82
TEC™15	0.35	5.6	21	0.53		15.1	85	83
Asahi U™	0.90	2.2	32	0.88		9.8		

d: film thickness; n: charge carrier concentration; μ: charge carrier mobility; ρ: bulk resistivity; R_{sh}: sheet resistance; $T_{\lambda,550}$: transmittance at 550 nm; $T_{\lambda,400-700}$: average transmittance over visible light range, 400–700 nm.

For all other samples synthesised, the typical morphologies observed are shown, Fig. 3b) and c). The increase in fluorine concentration did lead to a change in crystallite size and shape, Fig. 3d), with samples synthesised from 30 mol% F solutions all showing a larger range of grain sizes than their 15 mol% F analogues. Apart from this, however, there is little difference in the surface morphology of the deposited films, with all films displaying pyramidal-like particles, which are indicative of F-doped SnO_2 films grown by AACVD [5,24].

To determine how the surface roughness was affected by the change in precursor concentration, atomic force microscopy (AFM) measurements were taken, Fig. 4. As shown, there is little difference in the surface roughness on increasing the Sn concentration from 1 mol dm^{-3} to 2 mol dm^{-3} and the fluorine concentration has little impact on the surface roughness values either, with 15 and 30% F-doping (mol%) showing a similar surface morphology. Root mean square roughness (RMS) values ranged between 19.22 and 21.80 nm. The crystallite sizes and shapes present in the AFM images match well with those found in the SEM images, Fig. 3. The AFM measurements suggest that the increase in either Sn or F concentration does not affect the surface morphology, with the electrical properties observed being dependent on how well the fluorine is incorporated into the SnO_2 lattice. High surface roughness is one way in which to increase light scattering for solar cell applications, so being able to deposit rough surfaces with high growth rates is of benefit for this application [33,34].

X-ray photoelectron spectroscopy (XPS) was used to probe the oxidation states of Sn and O and the level of incorporation of F in the samples synthesised. Typical spectra for surface and bulk species of Sn and O are shown in Fig. 5. In all cases, only Sn^{4+} was observed for all samples, with the binding energy for the $Sn3d_{5/2}$ peak being at 487.0 eV which matched literature values for SnO_2 (± 0.2 eV) [35,36].

The surface O1s scan, Fig. 5b, showed a mix of O—Sn, O—C and O—H environments, the O—H signal is attributed to adsorbed water and the O—C to surface carbon, both of these signals decreased upon etching of the films, with only O—Sn detectable after 60 s of etching (~10 nm etched into the film). With further etching, up to 400 s (~55 nm etched into the film), no further observable change was noticed in either the O1s or Sn3d environments. The O—Sn binding energy was at 530.6 eV, which matched literature values for SnO_2 (± 0.2 eV) [37].

The F1s region was scanned to determine the fluorine environment present in the samples and fluorine concentration was then determined by comparing the area of the F1s peak against the Sn3d peak (once relative sensitivity factors had been applied). The fluorine 1s data was noisy (spectra shown in supporting information), indicating that there was a low concentration of fluorine in the samples. The peaks were generally centred around 648.8 eV, this is within 0.3 eV of other literature values for F-doped SnO_2 [5,27].

To determine whether the fluorine was uniformly distributed throughout the films, the samples were etched and the F1s region was scanned in detail. The F:Sn ratio, after correcting for relative sensitivity of F1s and Sn3d, was compared to determine whether the fluorine was uniformly distributed. From this data, it was determined that the concentration of fluorine in the films was consistent throughout the film from surface to bulk. There was no obvious surface segregation of the fluorine in any of the samples. The at.% of fluorine in the samples was between 0.5 and 1% for all films produced. This level of fluorine incorporation did not change upon altering the Sn concentration from 0.2 to 2.0 mol dm^{-3}, showing that aerosol assisted CVD methods can reliably reproduce film properties as the growth rates are increased. Interestingly, the fluorine incorporation was higher for the 15% F:SnO_2 samples than the 30% F:SnO_2 samples. This suggests that there is a relationship between the amount of fluorine in solution and the proportion incorporated into the SnO_2 lattice, with high levels of fluorine in solution leading to lower fluorine incorporation into the crystal lattice. This could indicate that there is a solubility limit for fluorine in the precursor solution. The incorporation of fluorine into the deposited films was always significantly lower than present in precursor

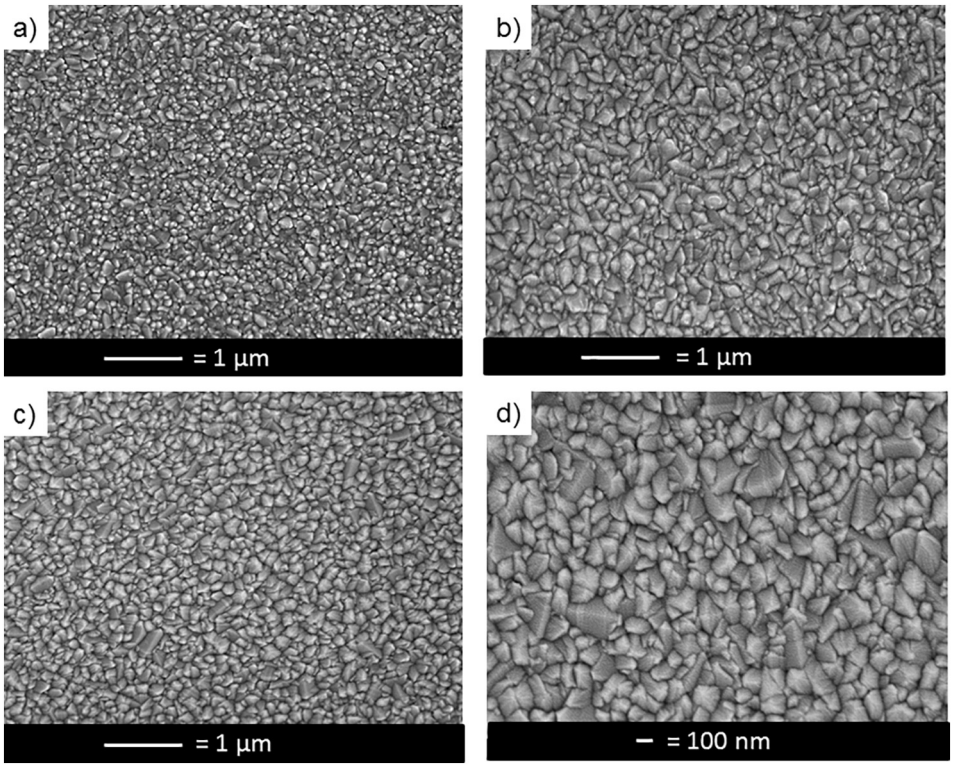

Fig. 3. Typical SEM images for a) sample 2, b) sample 6, c) sample 7 and d) sample 8. All samples synthesised by AACVD at 550 °C, using compressed air as the carrier gas. Full sample descriptions can be found in Table 1.

solution, suggesting that the fluorine is predominantly reacting to form waste products. As the tin precursor contains carbon and the C—F bond being energetically favourable, this could be the cause for the low level of fluorine incorporation in the deposited films.

Although fluorine was detected within the XPS data, the signal was very weak with a high noise to signal ratio- this leads us to consider that the at.% of fluorine in the sample is below 1%, this is the threshold of reliable detection for XPS. Therefore, although the fluorine can be detected and can be seen in both the UV/vis and Hall effect data, the measured values cannot be included as the error on these would be larger than the value calculated from the XPS data.

3.2. Functional testing

To determine the conductivity of the films, Hall effect measurements were obtained for all samples. These are summarised in Table 2. All samples showed good visible light transmission of around 80%, although the best films for electrical conductivity had lower overall visible light transmission. This could be improved by the inclusion of anti-reflection coatings to bring these films to above 80% transmission between 400 and 700 nm [38,39].

Electrical conductivity data showed a trend with increasing Sn concentration in the precursor solution, where increasing from 0.2 to 1.0 mol dm^{-3} led to a significant reduction in both resistivity values (ρ) and sheet resistances (R_{Sh}). The most dramatic decrease was seen for the 15% F:SnO_2 (by vol.) samples, where the sheet resistance decreased by 3 orders of magnitude, from ~1740 to ~7 $\Omega\square^{-1}$. The deposition time for these samples was fixed at 5 min, which is 6 to 8 times faster than typical aerosol assisted CVD methods [40–42], but still achieving excellent electrical and optical properties, which shows that aerosol assisted CVD can deliver highly uniform conformal coatings whilst maintaining excellent functional properties in the deposited films.

When the concentration of fluorine in solution was doubled, to 30%, in general there was an improvement in the electrical conductivity of the synthesised samples. This gave the lowest sheet resistance of 5.3 $\Omega\square^{-1}$ for the sample deposited from the 1.0 mol dm^{-3} precursor solution with 30% vol. F, which is lower than values quoted for common industrial FTO thin films (as shown in Table 2). This also demonstrates that aerosol assisted chemical vapour deposition methods can be scaled-up whilst maintaining excellent visible light transmission and electrical conductivity. The limiting factor for increasing depositions growth rates being the ability to aerosol viscous solutions. This also shows that tailoring of the processes can be easily achieved by simple changes to precursor concentrations in solution - which is of benefit as processes such as atmospheric pressure CVD are much more difficult to achieve this level of control due to the need to determine the mass flow rates from vapour pressures of volatile precursors.

As X-ray photoelectron spectroscopy is only sensitive to around 1 at.%, so although it was possible to determine that fluorine had been incorporated in all samples, determining the exact at.% was not possible. The lattice parameters, however, do give an indication of differing fluorine incorporation due to the differences in the calculated lattice parameters, as shown Table 1. This is also supported by the UV/vis spectra, which show that the samples 5 and 6 have the highest reflectivity in near IR wavelengths, once again indicative of higher fluorine doping. This suggests that although the fluorine incorporation is low, very small differences in F at.% can have dramatic changes on the properties of the films. Furthermore, samples 5 and 6 also had the highest number of charge carriers of any of the deposited films with both of these having double the number of charge carriers of the next best performing films, giving further evidence that there was a difference in fluorine doping into the deposited films.

The effect of fluorine incorporation, into the SnO_2 lattice, on the properties of the resultant FTO thin films can be seen by comparison of the films deposited from 1.0 and 2.0 mol dm^{-3} tin (with 15 mol% F). Both of these films had a thickness of around 500 nm (± 20) and so differences in electrical properties can only be attributed to film morphology and incorporation of fluorine into the structure. The XRD patterns, Fig. 1a, for these samples show that the films deposited from the 1.0 mol dm^{-3} solution had a greater preferential orientation

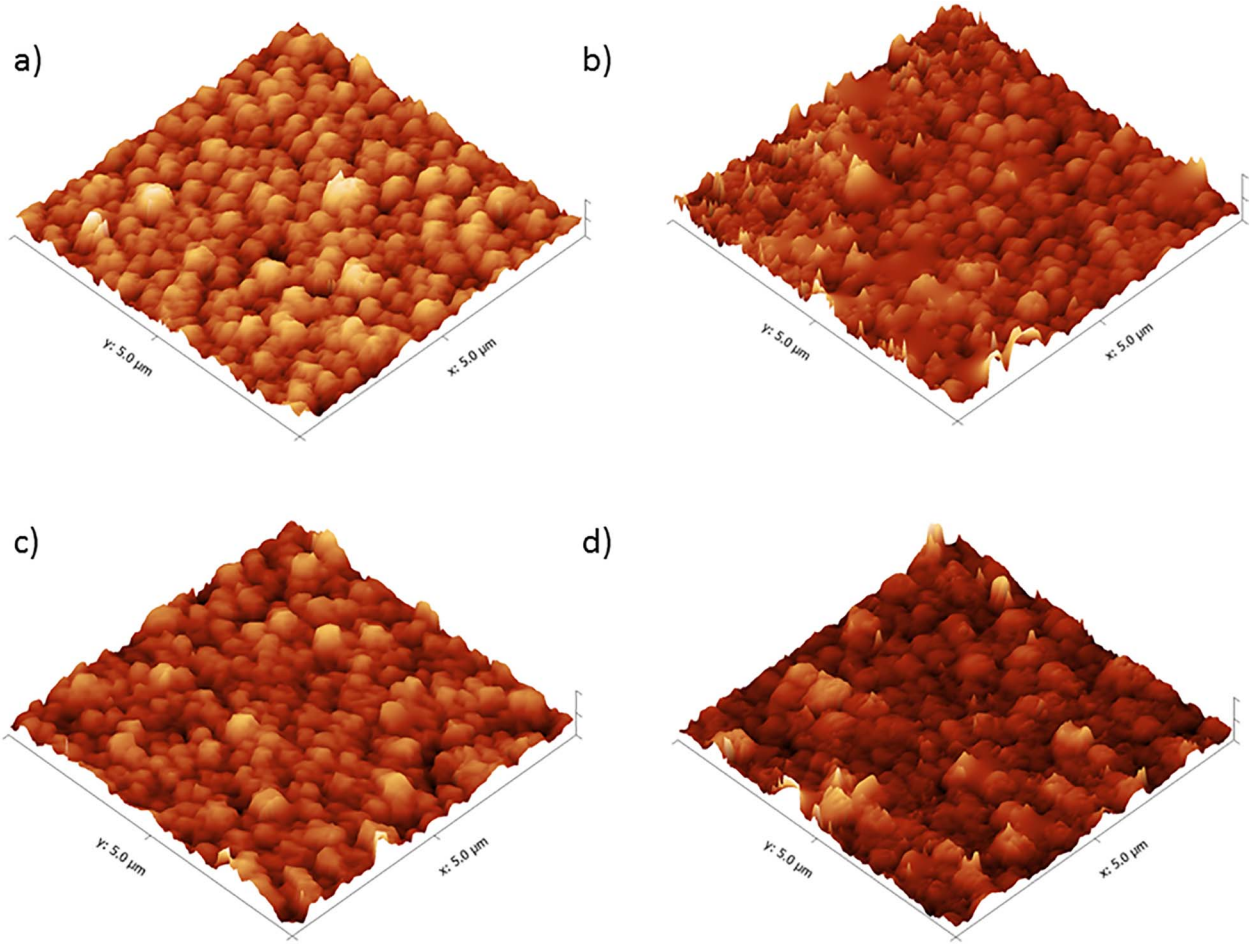

Fig. 4. AFM images for samples a) sample 5 b) sample 6 c) sample 7 and d) sample 8. The root mean square roughness varied between 19.22 and 21.80 nm for the samples shown. The z-axis scale is 0.25 µm for all AFM images. Sample descriptions can be found in Table 1. For all images, a scale factor of 4 was used for the z axis. All samples synthesised by AACVD at 550 °C, using compressed air as the carrier gas.

towards the (200) diffraction peak when compared to the films deposited from the 2.0 mol dm^{-3} solution. The (200) diffraction peak has been shown to be favoured by fluorine incorporation into the SnO_2 crystal lattice, with higher incorporation leading to greater preferential orientation [5,43,44]. The same relationship is seen for samples synthesised from solutions of 30% F 1.0 mol dm^{-3} and 30% F 2.0 mol dm^{-3}. Elangovan et al. have also seen a similar relationship with FTO films grown by spray pyrolysis [45].

Doubling the F:Sn ratio in the precursor solution had a dramatic effect on the electrical resistivity for the 0.2 mol dm^{-3} samples. As Table 2 shows, sample 2 had a sheet resistance of 300.4 $\Omega\square^{-1}$, whereas sample 1 had a higher sheet resistance of 1738.7 $\Omega\square^{-1}$. This was not the case for concentrations above, where each pair of samples synthesised at the same Sn concentration but different F concentrations, such as samples 5 and 6, showed very similar electrical resistivity values.

The results from the use of the collision atomiser show that there is a clear relationship between the initial concentration of the precursors in solution and the properties of the deposited film. This relationship shows that increasing the concentration of precursors in solution leads to better electrical properties with little loss in optical transmission. The main drawback of the collision atomiser is the ability to generate a mist from highly viscous solutions; this is evident from the stalling of film growth rates when the precursor concentration is above 1 mol dm^{-3}. This can be overcome by using a different method to develop the aerosol from the precursor solution, such as a piezoelectric nozzle to generate the precursor mist.

The film growth rates shown here of up to 100 nm min^{-1}, coupled with the electrical properties that exceed typical commercial standards and visible light transmission above 78% all show that aerosol assisted CVD methods can be scaled without loss of desired functionality in the deposited films. Furthermore, the solution chemistry can also be easily tailored to further enhance the properties displayed by the synthesised materials. This shows the great potential of aerosol assisted CVD methods to be used for industrial processes allowing access to a greater range of precursors. Aerosol assisted CVD is also performed at atmospheric pressure, which means that it can be integrated into current industrial processes without the need for extensive modifications or high vacuum conditions.

Aerosol assisted CVD techniques have been previously used to synthesise a large range of functional materials including; TCO materials, such as, doped ZnO [11,46,47], W-doped TiO_2 [48] and ITO; [42,49] photocatalysts; [50–52] solar cell materials; [53] gas sensing [41,54] and photo-chromic materials [55]. With such a wide-range of functional materials open to aerosol assisted routes, being able to scale-up the synthesis whilst maintaining the ease of control over doping, stoichiometry and availability of a wide range of starting precursors is of paramount significance. The results presented here are a key step to proving the ability of aerosol assisted methods to be able to show enhanced growth rates whilst still delivering high quality materials.

4. Conclusions

Aerosol assisted chemical vapour deposition has been successfully shown to be able to be scaled from ~10 nm min^{-1} to ~100 nm min^{-1}

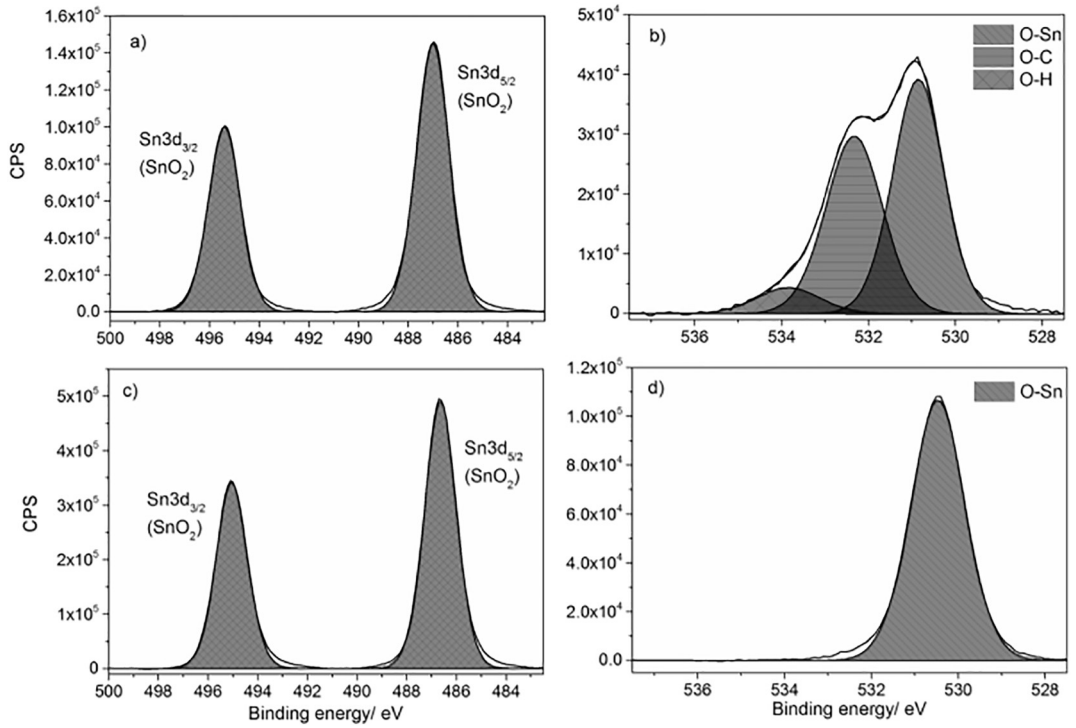

Fig. 5. Typical XPS spectra for surface (Fig. 5a and b) and bulk (Fig. 5c and d) Sn and O species present in FTO films deposited by AACVD from $^{n}BuSnCl_3$ and NH_4F in methanol at 550 °C (compressed air as carrier gas).

by increasing the concentration of the precursors in solution. This can be related to mass flow rates, as the solution concentration is increased, there are a greater number of molecules of Sn and F precursors passing through the reactor each minute, meaning that there is more of the desired material available for reaction and film growth. The thin films of FTO deposited were shown to have excellent electrical properties and visible light transmission of ~80% which is the benchmark for industrial coatings of TCO materials. The results were able to demonstrate the ability of aerosol assisted synthesis to give precise control over doping of materials, due to the solution based approach. This synthesis route gives the possibility of delivering on-line high-throughput synthesis of industrially important materials and also for the use of a far greater range of precursors and dopants, opening up a large range of potential new material syntheses.

Author contributions

M.J.P., D.B.P. and R.L.W contributed experimental and characterisation techniques, J.A.D, I.P.P. and C.J.C. supervised the work, all authors contributed to writing the manuscript.

Competing financial interests

The authors declare no competing financial interests.

Acknowledgements

The authors would like to thank the EPSRC for grant EP/L017709 and a studentship (R.L.W.) and UCL for an impact studentship (D. B. P.).

References

[1] M.R. Leyden, L.K. Ono, S.R. Raga, Y. Kato, S. Wang, Y. Qi, High performance perovskite solar cells by hybrid chemical vapor deposition, J. Mater. Chem. A 2 (2014) 18742–18745.
[2] M. Liu, M.B. Johnston, H.J. Snaith, Efficient planar heterojunction perovskite solar cells by vapour deposition, Nature 501 (2013) 395–398.
[3] D.J. Lewis, P. O'Brien, Ambient pressure aerosol-assisted chemical vapour deposition of (CH 3 NH 3) PbBr 3, an inorganic–organic perovskite important in photovoltaics, Chem. Commun. 50 (2014) 6319–6321.
[4] P. Marchand, I.A. Hassan, I.P. Parkin, C.J. Carmalt, Aerosol-assisted delivery of precursors for chemical vapour deposition: expanding the scope of CVD for materials fabrication, Dalton Trans. 42 (2013) 9406–9422.
[5] N. Noor, I.P. Parkin, Enhanced transparent-conducting fluorine-doped tin oxide films formed by aerosol-assisted chemical vapour deposition, J. Mater. Chem. C 1 (2013) 984–996.
[6] M.J. Powell, R. Quesada-Cabrera, A. Taylor, D. Teixeira, I. Papakonstantinou, R.G. Palgrave, G. Sankar, I.P. Parkin, Intelligent multifunctional VO2/SiO2/TiO2 coatings for self-cleaning, energy-saving window panels, Chem. Mater. 28 (2016) 1369–1376.
[7] I.P. Parkin, R.G. Palgrave, Self-cleaning coatings, J. Mater. Chem. 15 (2005) 1689–1695.
[8] C.R. Crick, J.C. Bear, A. Kafizas, I.P. Parkin, Superhydrophobic photocatalytic surfaces through direct incorporation of titania nanoparticles into a polymer matrix by aerosol assisted chemical vapor deposition, Adv. Mater. 24 (2012) 3505–3508.
[9] V.A. Ganesh, H.K. Raut, A.S. Nair, S. Ramakrishna, A review on self-cleaning coatings, J. Mater. Chem. 21 (2011) 16304–16322.
[10] K. Minegishi, Y. Koiwai, Y. Kikuchi, K. Yano, M. Kasuga, A. Shimizu, Growth of p-type zinc oxide films by chemical vapor deposition, Jpn. J. Appl. Phys. 36 (1997) L1453.
[11] D.S. Bhachu, G. Sankar, I.P. Parkin, Aerosol assisted chemical vapor deposition of transparent conductive zinc oxide films, Chem. Mater. 24 (2012) 4704–4710.
[12] K.-L. Ou, D. Tadytin, K.X. Steirer, D. Placencia, M. Nguyen, P. Lee, N.R. Armstrong, Titanium dioxide electron-selective interlayers created by chemical vapor deposition for inverted configuration organic solar cells, J. Mater. Chem. A 1 (2013) 6794–6803.
[13] M.J. Hampden-Smith, T.T. Kodas, Chemical vapor deposition of metals: part 1. An overview of CVD processes, Chem. Vap. Depos. 1 (1995) 8–23.
[14] G. Versteeg, P. Blauwhoff, W. Van Swaaij, The effect of diffusivity on gas-liquid mass transfer in stirred vessels. Experiments at atmospheric and elevated pressures, Chem. Eng. Sci. 42 (1987) 1103–1119.
[15] K. Choy, Chemical vapour deposition of coatings, Prog. Mater. Sci. 48 (2003) 57–170.
[16] X. Hou, K.L. Choy, Processing and applications of aerosol-assisted chemical vapor deposition, Chem. Vap. Depos. 12 (2006) 583–596.
[17] C.E. Knapp, C.J. Carmalt, Solution based CVD of main group materials, Chem. Soc. Rev. 45 (2016) 1036–1064.
[18] R.G. Palgrave, I.P. Parkin, Aerosol assisted chemical vapor deposition using nanoparticle precursors: a route to nanocomposite thin films, J. Am. Chem. Soc. 128 (2006) 1587–1597.
[19] C. Chew, P. Bishop, C. Salcianu, C.J. Carmalt, I.P. Parkin, Aerosol-assisted deposition of gold nanoparticle-tin dioxide composite films, RSC Adv. 4 (2014) 13182–13190.
[20] C.S. McNally, D.P. Turner, A.N. Kulak, F.C. Meldrum, G. Hyett, The use of cationic surfactants to control the structure of zinc oxide films prepared by chemical vapour

deposition, Chem. Commun. 48 (2012) 1490–1492.
[21] N. Yamada, M. Yamada, H. Toyama, R. Ino, X. Cao, Y. Yamaguchi, Y. Ninomiya, High-throughput optimization of near-infrared-transparent Mo-doped In2O3 thin films with high conductivity by combined use of atmospheric-pressure mist chemical-vapor deposition and sputtering, Thin Solid Films 626 (2017) 46–54.
[22] C. Edusi, G. Hyett, G. Sankar, I.P. Parkin, Aerosol-assisted CVD of titanium dioxide thin films from methanolic solutions of titanium tetraisopropoxide; substrate and aerosol-selective deposition of rutile or anatase, Chem. Vap. Depos. 17 (2011) 30–36.
[23] N.P. Chadwick, S. Sathasivam, S.M. Bawaked, M. Mokhtar, S.A. Althabaiti, S.N. Basahel, I.P. Parkin, C.J. Carmalt, The use of time resolved aerosol assisted chemical vapour deposition in mapping metal oxide thin film growth and fine tuning functional properties, J. Mater. Chem. A 3 (2015) 4811–4819.
[24] D.S. Bhachu, M.R. Waugh, K. Zeissler, W.R. Branford, I.P. Parkin, Textured fluorine-doped tin dioxide films formed by chemical vapour deposition, Chem. Eur. J. 17 (2011) 11613–11621.
[25] A. Kafizas, C. Crick, I.P. Parkin, The combinatorial atmospheric pressure chemical vapour deposition (cAPCVD) of a gradating substitutional/interstitial N-doped anatase TiO2 thin-film; UVA and visible light photocatalytic activities, J. Photochem. Photobiol. A Chem. 216 (2010) 156–166.
[26] A. Moholkar, S. Pawar, K. Rajpure, C. Bhosale, J. Kim, Effect of fluorine doping on highly transparent conductive spray deposited nanocrystalline tin oxide thin films, Appl. Surf. Sci. 255 (2009) 9358–9364.
[27] N. Noor, I.P. Parkin, Halide doping effects on transparent conducting oxides formed by aerosol assisted chemical vapour deposition, Thin Solid Films 532 (2013) 26–30.
[28] V. Consonni, G. Rey, H. Roussel, D. Bellet, Thickness effects on the texture development of fluorine-doped SnO2 thin films: the role of surface and strain energy, J. Appl. Phys. 111 (2012) 033523.
[29] J. Suffner, P. Ágoston, J. Kling, H. Hahn, Chemical vapor synthesis of fluorine-doped SnO2 (FTO) nanoparticles, J. Nanopart. Res. 12 (2010) 2579–2588.
[30] H. Ma, D. Zhang, Y. Chen, S. Li, J. Ma, F. Zong, Large scale fluorine doped textured transparent conducting SnO 2 films deposited by atmospheric pressure chemical vapour deposition, Thin Solid Films 298 (1997) 151–155.
[31] E. Elangovan, K. Ramamurthi, Studies on micro-structural and electrical properties of spray-deposited fluorine-doped tin oxide thin films from low-cost precursor, Thin Solid Films 476 (2005) 231–236.
[32] G.A. Kumara, C.K. Ranasinghe, E.N. Jayaweera, H.N. Bandara, M. Okuya, R.G. Rajapakse, Preparation of fluoride-doped tin oxide films on soda–lime glass substrates by atomized spray pyrolysis technique and their subsequent use in dye-sensitized solar cells, J. Phys. Chem. C 118 (2014) 16479–16485.
[33] Z. Fang, H. Zhu, Y. Yuan, D. Ha, S. Zhu, C. Preston, Q. Chen, Y. Li, X. Han, S. Lee, Novel nanostructured paper with ultrahigh transparency and ultrahigh haze for solar cells, Nano Lett. 14 (2014) 765–773.
[34] H. Yates, P. Evans, D. Sheel, S. Nicolay, L. Ding, C. Ballif, High-performance tandem silicon solar cells on F: SnO 2, Surf. Coat. Technol. 230 (2013) 228–233.
[35] W.-K. Choi, J.-S. Cho, S.-K. Song, H.-J. Jung, S.-K. Koh, Auger electron and X-ray photoelectron spectroscopy studies of oxidation of tin using SnOx thin films grown by reactive ion-assisted deposition, Jpn. J. Appl. Phys. 35 (1996) 5820.
[36] F. Vicent, E. Morallo, C. Quijada, J. Va, A. Aldaz, F. Cases, Characterization and stability of doped SnO2 anodes, J. Appl. Electrochem. 28 (1998) 607–612.
[37] A. Christie, J. Lee, I. Sutherland, J. Walls, An XPS study of ion-induced compositional changes with group II and group IV compounds, Appl. Surf. Sci. 15 (1983) 224–237.
[38] H.K. Raut, S.S. Dinachali, K.K. Ansah-Antwi, V.A. Ganesh, S. Ramakrishna, Fabrication of highly uniform and porous MgF2 anti-reflective coatings by polymer-based sol–gel processing on large-area glass substrates, Nanotechnology 24 (2013) 505201.
[39] H.K. Raut, A.S. Nair, S.S. Dinachali, V.A. Ganesh, T.M. Walsh, S. Ramakrishna, Porous SiO 2 anti-reflective coatings on large-area substrates by electrospinning and their application to solar modules, Sol. Energy Mater. Sol. Cells 111 (2013) 9–15.
[40] C. Piccirillo, R. Binions, I.P. Parkin, Nb-doped VO2 thin films prepared by aerosol-assisted chemical vapour deposition, Eur. J. Inorg. Chem. (2007) 4050–4055.
[41] S. Vallejos, P. Umek, T. Stoycheva, F. Annanouch, E. Llobet, X. Correig, P. De Marco, C. Bittencourt, C. Blackman, Single-step deposition of Au-and Pt-nanoparticle-functionalized tungsten oxide nanoneedles synthesized via aerosol-assisted CVD, and used for fabrication of selective gas microsensor arrays, Adv. Funct. Mater. 23 (2013) 1313–1322.
[42] C.E. Knapp, G. Hyett, I.P. Parkin, C.J. Carmalt, Aerosol-assisted chemical vapor deposition of transparent conductive gallium − indium − oxide films, Chem. Mater. 23 (2011) 1719–1726.
[43] C. Agashe, B.R. Marathe, M.G. Takwale, V.G. Bhide, Structural properties of SnO2: F films deposited by spray pyrolysis technique, Thin Solid Films 164 (1988) 261–264.
[44] M. Adnane, H. Cachet, G. Folcher, S. Hamzaoui, Beneficial effects of hydrogen peroxide on growth, structural and electrical properties of sprayed fluorine-doped SnO2 films, Thin Solid Films 492 (2005) 240–247.
[45] E. Elangovan, K. Ramamurthi, A study on low cost-high conducting fluorine and antimony-doped tin oxide thin films, Appl. Surf. Sci. 249 (2005) 183–196.
[46] D.B. Potter, D.S. Bhachu, M.J. Powell, J.A. Darr, I.P. Parkin, C.J. Carmalt, Al-, Ga-, and In-doped ZnO thin films via aerosol assisted CVD for use as transparent conducting oxides, Phys. Status Solidi A 213 (5) (2016) 1346–1352.
[47] M. Nolan, J. Hamilton, S. O'Brien, G. Bruno, L. Pereira, E. Fortunato, R. Martins, I. Povey, M. Pemble, The characterisation of aerosol assisted CVD conducting, photocatalytic indium doped zinc oxide films, J. Photochem. Photobiol. A Chem. 219 (2011) 10–15.
[48] S. Sathasivam, D.S. Bhachu, Y. Lu, N. Chadwick, S.A. Althabaiti, A.O. Alyoubi, S.N. Basahel, C.J. Carmalt, I.P. Parkin, Tungsten doped TiO2 with enhanced photocatalytic and optoelectrical properties via aerosol assisted chemical vapor deposition, Sci. Rep. 5 (2015).
[49] C.E. Knapp, A. Kafizas, I.P. Parkin, C.J. Carmalt, The use of combinatorial aerosol-assisted chemical vapour deposition for the formation of gallium-indium-oxide thin films, J. Mater. Chem. 21 (2011) 12644–12649.
[50] L. Romero, R. Binions, On the influence of DC electric fields on the aerosol assisted chemical vapor deposition growth of photoactive titanium dioxide thin films, Langmuir 29 (2013) 13542–13550.
[51] S. Ariffin, H. Lim, Z. Talib, A. Pandikumar, N. Huang, Aerosol-assisted chemical vapor deposition of metal oxide thin films for photoelectrochemical water splitting, Int. J. Hydrog. Energy 40 (2015) 2115–2131.
[52] N. Chadwick, S. Sathasivam, A. Kafizas, S.M. Bawaked, A.Y. Obaid, S. Al-Thabaiti, S.N. Basahel, I.P. Parkin, C.J. Carmalt, Combinatorial aerosol assisted chemical vapour deposition of a photocatalytic mixed SnO 2/TiO 2 thin film, J. Mater. Chem. A 2 (2014) 5108–5116.
[53] S. Lim, N.M. Huang, H.N. Lim, M. Mazhar, Surface modification of aerosol-assisted CVD produced TiO2 thin film for dye sensitised solar cell, Int. J. Photoenergy 2014 (2014).
[54] A.J. Naik, M.E. Warwick, S.J. Moniz, C.S. Blackman, I.P. Parkin, R. Binions, Nanostructured tungsten oxide gas sensors prepared by electric field assisted aerosol assisted chemical vapour deposition, J. Mater. Chem. A 1 (2013) 1827–1833.
[55] H. Kim, R.O. Bonsu, C. O'Donohue, R.Y. Korotkov, L. McElwee-White, T.J. Anderson, Aerosol-assisted chemical vapor deposition of tungsten oxide films and nanorods from oxo tungsten (VI) fluoroalkoxide precursors, ACS Appl. Mater. Interfaces 7 (2015) 2660–2667.